ELSEVIER

Composites Science and Technology 62 (2002) 1407–1414

COMPOSITES SCIENCE AND TECHNOLOGY

www.elsevier.com/locate/compscitech

A new mode I fracture test for composites with translaminar reinforcements

Leishan Chen, Bhavani.V. Sankar*, Peter.G. Ifju

Department of Aerospace Engineering, Mechanics and Engineering Science, University of Florida, PO Box 116250, Gainesville, FL 32611, USA

Received 4 September 2001; received in revised form 13 May 2002; accepted 14 May 2002

Abstract

A new test method is presented for Mode I delamination fracture toughness testing of laminated composites containing a high density of stitches or translaminar reinforcements. The test set up, which is similar to the standard Double Cantilever Beam test, induces an axial tension in the specimen in addition to the transverse forces responsible for propagation of delamination. The tensile stresses reduce the compressive stresses in the vicinity of the crack tip caused by the large bending moments required for crack propagation. The nonlinear differential equations of equilibrium of the new specimen are solved using an iterative procedure to obtain the strain energy release rate as a function of load and crack length. Experiments were conducted using carbon/epoxy specimens containing 6.2 stitches per square centimeter (40 stitches per square inch). Results include Mode I fracture toughness, crack tip bending moment, transverse deflection and slope as a function of crack length. It is found that the apparent fracture toughness of the specimens tested remains constant as the stitches break and crack propagates, and is about sixty times that of unstitched specimens.

Keywords: B. Fracture toughness; C. Delamination; Composites

1. Introduction

Laminated fiber composites, such as carbon-epoxy, have very high in-plane strength and stiffness, but they usually exhibit poor interlaminar strength and fracture toughness, and hence are vulnerable to delamination. One of the most effective ways of increasing interlaminar fracture toughness is through-the-thickness stitching. Stitching has numerous benefits for laminated composites. When the crack passes the stitches, stitches still hold the matrix and bridge the crack zone. Because stitches inherently resist any displacement between the delaminated sublaminates, the crack driving force at the delamination front is reduced. As more and more stitches become involved at the crack zone, the apparent fracture toughness of the composite increases. There are two forms of translaminar reinforcement: continuous and discontinuous. Both of them have been shown to significantly improve compression-after-impact strength [1–4], Modes I and II fracture toughness [1,2,5–7] and interlaminar shear strength [6]. Sharma and Sankar [1] found that stitching does not increase the impact load at which delamination begins to propagate, but greatly reduces the extent of delamination growth at the end of the impact event. This has also been confirmed by the analytical simulations performed by Sankar and Zhu [3]. Dexter and Funk [2] investigated the impact resistance and interlaminar fracture toughness of quasi-isotropic carbon-epoxy laminates made of unidirectional Thornel 300-6k fibers/Hercules 3501-6 resin and stitched with polyester or Kevlar yarns. The Mode I fracture toughness, characterized by the critical strain energy release rate, G_{IC}, was found to be about 30 times higher for the stitched laminates. Pelstring and Madan [4] developed semiempirical formulae relating damage tolerance of a composite laminate to stitching parameters. Mode I critical strain energy release rate was found to be 15 times greater than in unstitched laminates, and G_{IC} decreased exponentially with an increase in stitch spacing.

* Corresponding author. Tel.: +1-352-392-6749; fax: +1-352-392-7303.

E-mail address: sankar@ufl.edu (B.V. Sankar).

0266-3538/02/$ - see front matter
PII: S0266-3538(02)00096-9

Sharma and Sankar [1] found that the standard Mode I DCB test (ASTM Designation: D 5528-94a) is not suitable for specimens with high stitch density. The fracture toughness was so high that the specimens failed due to high compressive bending stresses before the crack propagated. A number of researchers [8–15] have tried to investigate the mechanisms of stitches in laminated composites, and some numerical and analytical methods were developed to predict the properties of stitched composites. But, for medium to high density stitched composites, they usually lack the experimental data to support their results. Chen et al. [16] developed an innovative fixture that applied a uniform tensile stress to the specimen, thus reducing the compressive stresses that caused the beam to fail in the vicinity of the crack-tip. In that fixture the specimen ends were attached to rollers that are constrained to move on a pair of inclined rails. This arrangement allowed application of a transverse force to open the crack and a tensile force to mitigate the effects of flexural compression. There were many disadvantages to the fixture. It was difficult to design a gripping mechanism to attach the rollers to the specimen. Further, friction between the rollers and the rails yielded higher values of fracture toughness. The fixture had many linkages increasing the overall compliance of the loading system, which may be a source of error.

In the present paper we describe a new fixture with a robust gripping mechanism for Mode I fracture testing of composite specimens with very high stitch density. An analytical method has been developed to analyze the specimen and compute the energy release rate for a given load and crack length. Experiments were conducted using carbon/epoxy composite with stitch densities as high as 6.2 stitches per square centimeter (40 stitches per square inch). It has been found that the Mode I fracture toughness can increase by a factor of 60 due to heavy stitching, and the present fixture is capable of testing such specimens.

2. Description of the new test fixture

The standard DCB specimen is depicted in Fig. 1. The energy release rate in the DCB specimen is given by $\frac{M^2}{bEI}$, where $M = Qa$ is the bending moment in one of the sublaminates at the crack tip, Q is the transverse force, a is the crack length, b is the width of the specimen and EI is the flexural rigidity of the sublaminates. As the fracture toughness of the material increases, larger bending moments are required to propagate the crack. The bending moments also produce large compressive stresses on the outer surfaces of the specimen as indicated in Fig. 1. Although fiber composites are strong in tension, their compressive strength is limited by fiber microbuckling, which causes the specimens to fail before the crack could propagate. One of the ways of reducing the compressive stresses is to apply a uniform tension in both arms of the DCB specimen. It should be noted that this tensile stress being equal in both arms does not contribute to the energy release rate, and Mode I crack propagation is maintained. Following this idea a new fixture has been developed as illustrated in Fig. 2. This fixture can supply forces along two directions. The transverse component of the force is for crack opening and the axial component is for applying the

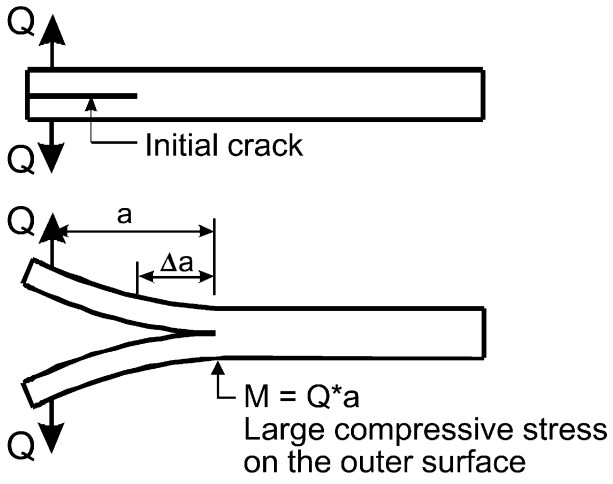

Fig. 1. The schematic standard DCB test setup.

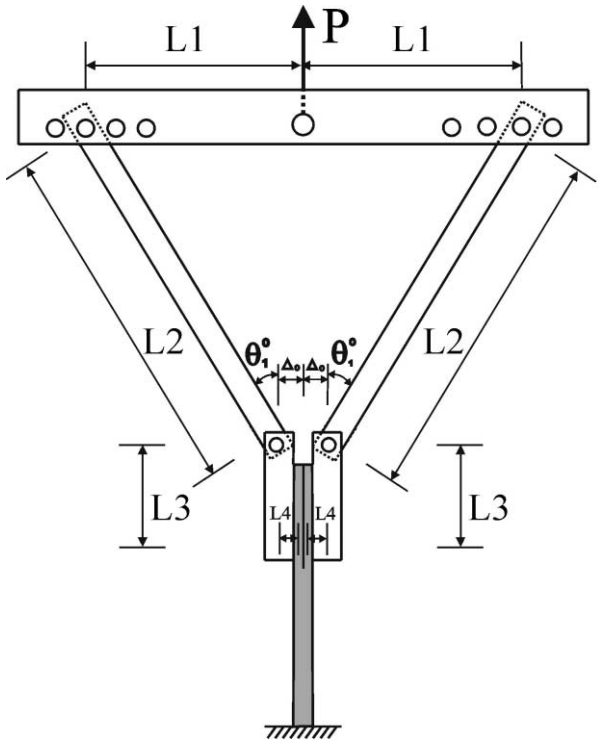

Fig. 2. The novel DCB test setup.

tensile force. The fixture has been designed such that the initial angles of the arms are adjustable and for a given stitched specimen, the optimal angle can be determined.

A challenge in the new fixture is the design of the specimen grips that can transmit both axial and transverse forces. Conventional method of bonding the tabs to the specimen does not work as the bonded tabs cannot withstand the large tensile and shear stresses caused by the larger load required to propagate the crack. A notch in the form of a circular arc was machined in the specimen ends as shown in Fig. 3. The notch surface forms a 45° angle to the specimen surface. A pair of adjustable grips that match the notch profile in the specimen were machined out of steel (Fig. 4). The final assembly of the specimen and the grips is shown in Fig. 5. Fig. 6 shows a series of pictures taken from one of the tests. The fixture unzips the stitches one by one and the crack propagation is found to be stable.

3. Analysis of the specimen

A schematic of the new DCB test set up and the free-body diagram of AB are shown in Fig. 7. As a row of stitches breaks, the crack front reaches the location of the next row of the stitches. The current crack tip is located at Point B, and the portion of the specimen in the grip (AC in Fig. 7) is considered rigid. All of the forces and the bending moment at A can be expressed as:

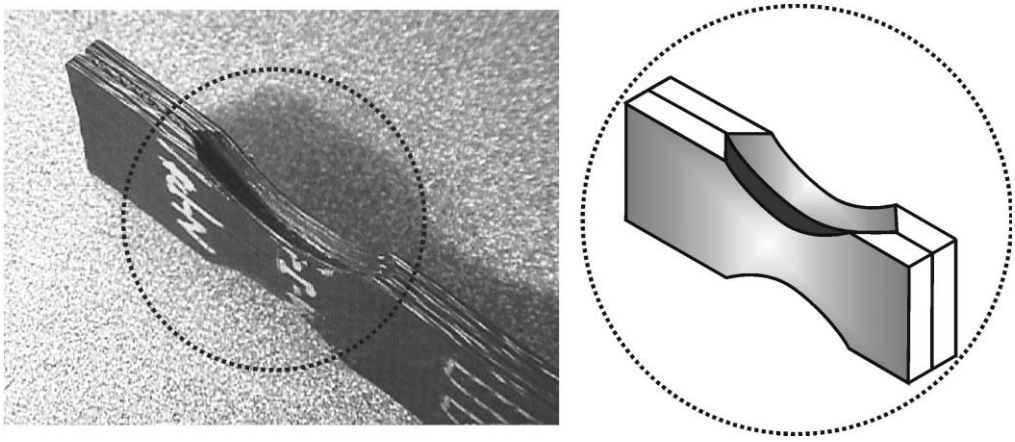

Fig. 3. The notches in the specimen.

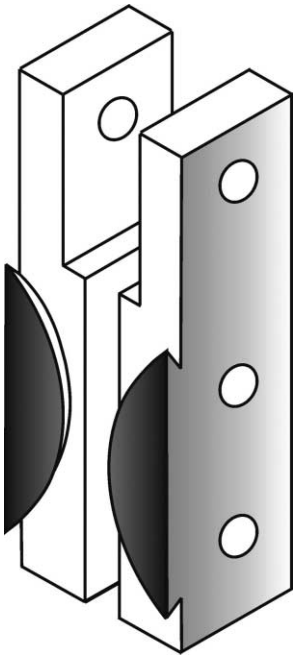

Fig. 4. Schematic of the specimen grips. Note that the specimen grips match the notches in the specimen shown in Fig. 3.

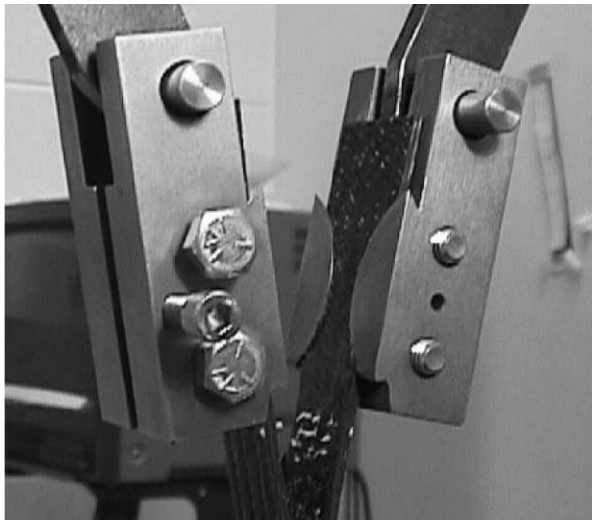

Fig. 5. A view of the assembled specimen.

$$F_A = F$$

$$M_A = F(L_3\cos\theta_2 - L_4\sin\theta_2)\sin\theta_1 - F(L_3\sin\theta_2 + L_4\cos\theta_2)\ \cos\theta_1 = FL_3\sin(\theta_1 - \theta_2) - FL_4\cos(\theta_1 - \theta_2) \tag{1}$$

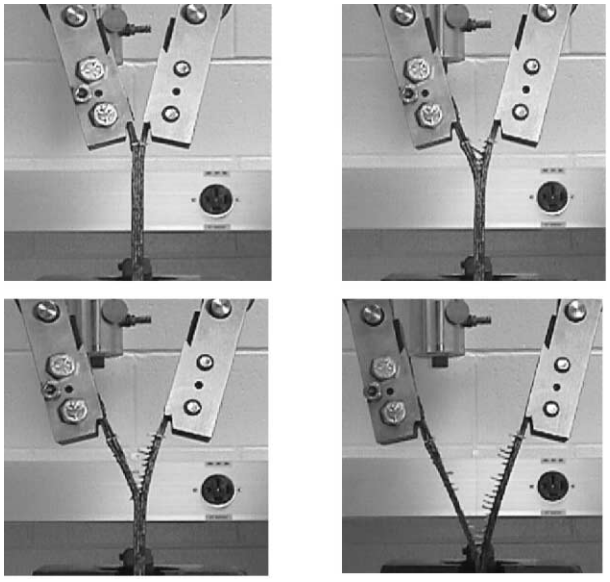

Fig. 6. A series of pictures taken during the new DCB test.

The angles θ_1 and θ_2 are indicated in Fig.7. The angle θ_2 is the slope at point A, i.e., $\theta_2 = \frac{\geq \mathrm{d}v(x)}{\mathrm{d}x}\Big|_{x=L_5}$. The angle θ_1 can be calculated using the following geometrical relations:

$$\Delta_A = \Delta_0 + L_3^*\sin\theta_2 + v_A, \qquad v_A = v(x)\big|_{x=L_5},$$
$$\theta_1 = \sin^{-1}\left(\frac{L_1 - \Delta_A}{L_2}\right), \tag{2}$$

where the distance Δ_0 is indicated in Fig. 2.

We only need to analyze the portion AB as shown in Fig 7. The expression for the bending moment $M(x)$ can be derived as:

$$\begin{aligned} M(x) &= M_A + F(L_5 - x)\sin\theta_1 - F\cdot[v_A - v(x)]\cdot\cos\theta_1 \\ &= FL_3\sin(\theta_1 - \theta_2) - FL_4\cos(\theta_1 - \theta_2) \\ &\quad + F(L_5 - x)\sin\theta_1 - F\cdot[v_A - v(x)]\cdot\cos\theta_1 \end{aligned} \tag{3}$$

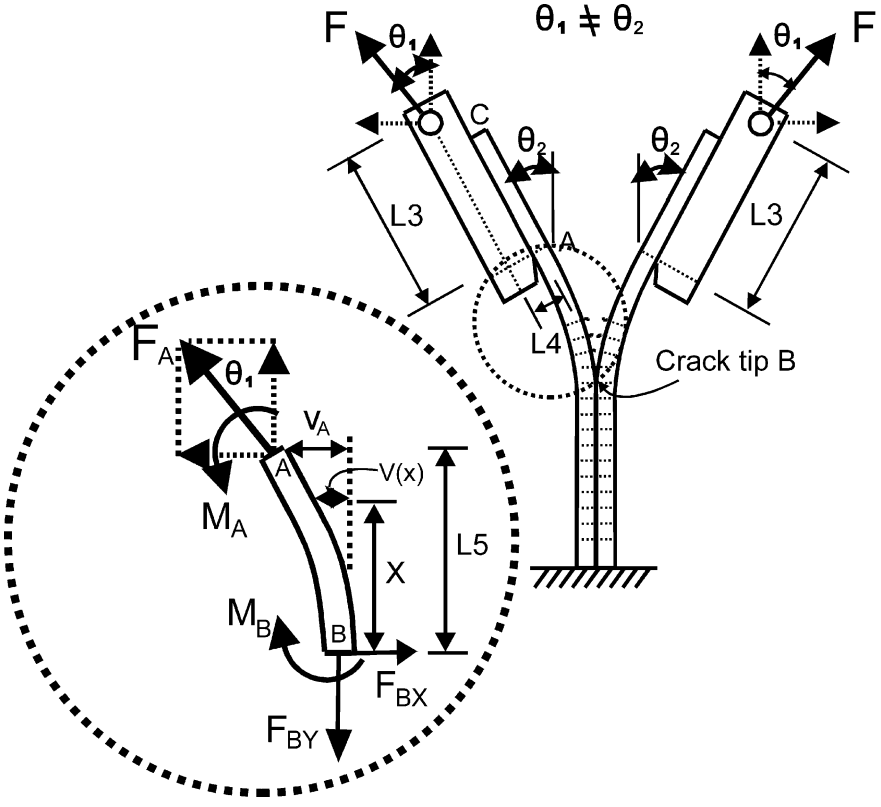

Fig. 7. Schematic of the new DCB test setup and free body diagram AB of a specimen.

where v_A and $v(x)$ are transverse deflections at cross section A and an arbitrary cross section at x. It must be mentioned that the calculation of bending moment $M(x)$ in Eq. (3) is exact, and the contribution of the axial force to the bending moment due to large deflection is included. The governing differential equation for the beam is:

$$\frac{1}{\left(1+(\mathrm{d}v/\mathrm{d}x)^2\right)^{3/2}}\frac{\mathrm{d}^2v(x)}{\mathrm{d}x^2}=\frac{1}{(1+\theta^2)^{3/2}}\frac{\mathrm{d}\theta}{\mathrm{d}x}=\frac{M(x)}{EI} \tag{4}$$

Where EI is the equivalent flexural rigidity of one arm of the specimen and the expression on the left hand side of the equation is exact for the beam curvature. At this point we make the usual approximation for the curvature:

$$\frac{\mathrm{d}^2v(x)}{\mathrm{d}x^2}=\frac{\mathrm{d}\theta}{\mathrm{d}x}=\frac{M(x)}{EI} \tag{5}$$

From the experiments (see Fig. 6) we noted that the slope of the beam is higher towards the tip of the DCB specimen where the bending moments are small. On the other hand, towards the crack tip, where the bending moment is large, the slopes are indeed small. Hence we are justified in neglecting the higher order term in the denominator for the curvature and this further simplifies the calculations.

The equivalent flexural rigidity EI was measured from a three-point bending test in which the maximum deflection δ at the center was related to the applied force P by $\delta = PL^3/48EI$ where L is the span of the loading fixture. The bending moment $M(x)$ is not only the function of x, but also the function of θ_1 and θ_2. An iterative numerical method was used to solve Eq. (5). The load F and the crack length L_5 are obtained from the test data. First the initial values of θ_1, θ_2 and v_A are calculated for the initial position of the specimen and Eq. (5) was solved for $v(x)$. After the first iteration, new values of θ_1, θ_2 and v_A were calculated and used for the second round of the iteration. As the relative errors between successive sets of values of θ_1, θ_2 and v_A become less than an allowable minimum, say 2%, the iterations are stopped, and the final numerical values are taken as the solution. Following are steps used in the iterative process:

Step 1: import F (load), L_5 (crack length) from the test.
Step 2: use the initial values of θ_1, θ_2 and v_A to solve $v(x)$.
Step 3: from $v(x)$, obtain new θ_1, θ_2 and v_A.
Step 4: calculate the relative errors between new θ_1, θ_2 and v_A and previous θ_1, θ_2 and v_A. If the errors are allowable, stop and output new θ_1, θ_2 and v_A as the final values of θ_1, θ_2 and v_A. Otherwise, go to step 2 by using new θ_1, θ_2 and v_A as input to calculate $v(x)$.

From the results, the bending moment and shear force at the section just behind the crack tip can be calculated for a given load and crack length. The energy release rate is obtained from the formula:

$$G_{\mathrm{IC}}=\frac{1}{b}\left(\frac{M^2}{EI}\right) \tag{6}$$

where b is the width of the specimen and M is the crack tip bending moment at the instant of crack propagation. It should be noted that in order to use the aforementioned iterative method, we need to measure the crack length corresponding to the peak load in the tests.

It must be mentioned that the aforementioned approach ignores the crack bridging effects caused by the unbroken stitches in the wake of the crack tip. Such crack bridging effects in stitched composites have been considered in great detail by Massabo and Cox [17]. Sankar and Dharmapuri [8] also analytically studied the effects of bridging in stitched composite beams. In the present study there are two reasons for ignoring the bridging effects (small scale bridging). First one is that the size of the bridging zone is small compared to the length of the crack. Typically it was about one stitch spacing, that is, at any given time not more than two unbroken stitches were found behind the crack tip. The second reason is that this bridging zone was found to be a constant as the crack tip moved forward. That is, there was no crack resistance effects and the fracture toughness remains constant with the crack length. Hence the present approach can be considered as a method of determining the apparent fracture toughness of the stitched composites where the micromechanics of stitch failure are not considered in detail.

4. Results and discussion

There are two methods of determining G_{IC} from the DCB tests. In the area method the work done by the external forces on the specimen is calculated from the area enclosed by the load-deflection diagram. This work is divided by the area of crack extension to obtain the average G_{IC}. We did not use this method as the specimen could not be unloaded completely because of the protruding broken stitches on the delamination surfaces. These stitches prevented complete closure of the two ligaments of the DCB specimen. Hence it was decided to use the formula $G_{\mathrm{IC}}=\frac{M^2}{bEI}$ where M is the crack tip bending moment at the instant of crack propagation. The value of G_{IC} calculated using this method can also be thought of as the instantaneous fracture toughness at the time of crack propagation. However, we need to know the bending moment at the crack tip from the load, crack length and other geometrical information. This is much simpler in conventional DCB specimens

and can be obtained as the product of the load and the crack length. In the current specimen we need to perform an analysis to obtain the bending moment. The main difference is the effect of the axial force on the bending moment, which now is a function of the transverse deflection of the specimen. This necessitates an iterative procedure to solve for the deflection of the beam. The analysis procedure is described in the following.

The specimens were cut from a panel which is made of 4 stacks of Saertex@ textile. Each stack is made of 7 layers with fiber orientations given by [45°/−45°/0°/90°/0°/−45°/45°]. The linear density of the Kevlar stitch is 1600 denier. The specimen is 19.1 cm (7.5 in) long and 2.0 cm (0.8 in) wide. A sample load-deflection diagram is shown in Fig. 8. As the stitches start breaking, one can note the fluctuations in the load and the saw-tooth like pattern of the load-deflection diagram. Each peak in the load corresponds to the breaking of one row of stitches. In the beginning the load to break the stitches increases (stitches 1–10), then a steady state is reached and the stitches break at a constant peak load. The twenty peak loads shown in Fig. 8 match the twenty rows of broken stitches. After carefully observing the specimen, we found that as one row of stitches broke, the crack front reached the next row of stitches. After measuring the distance between the initial position of the crack tip and the location of $(n+1)^{\text{th}}$ row of stitches, we can obtain the crack extension corresponding to n^{th} peak load. This peak load and the corresponding crack length (L_5) were used as the input data in Eq. (3)

The dimensions of the fixture, the specimen and the gripping area for a particular specimen (Figs. 2 and 7) were as follows: $L_1 = 190$ mm, $L_2 = 370$ mm, $L_3 = 57.8$ mm, $L_4 = 11$ mm, $L_5 = 15.6$ mm (the crack length corresponding to the first peak load of $P_1 = 3176$ N),

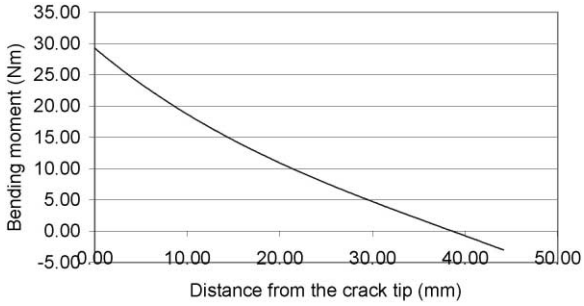

Fig. 9. Bending moment distribution along one arm of the DCB specimen for a crack length of 44.2 mm and load of 5420 N.

$b = 19.05$ mm (width of the specimen), $h = 2.98$ mm (the half of the thickness of the specimen). The initial values of θ_1, θ_2 and v_A (the specimen in the initial position) were 28.58°, 0° and 0, respectively. The equivalent Young's modulus of the specimen is equal to 44.42 GPa. After seven iterations, θ_1, θ_2 and v_A were equal to 26.9°, 8.8° and 1.36 mm, respectively. The relative errors of θ_1, θ_2 and v_A compared to the values of sixth iteration were 1.8, 1.7 and 1.2%, respectively.

By using the experimentally measured critical load and crack length AB, the bending moment, transverse displacement and slope along the AB can be determined by using the analytical method. For instance, we selected the tenth peak load (load = 5420 N) and measured the location of the eleventh row of stitches to obtain the crack length ($AB = 44.2$ mm). Figs. 9–11 show the bending moment, the deflection and the slope along the specimen length AB. One can note that the crack tip suffers the largest bending moment. If no axial forces were applied, the specimen would undergo micro-buckling in the vicinity of the crack-tip for this amount of the bending moment. However, an axial force of 2710 N significantly

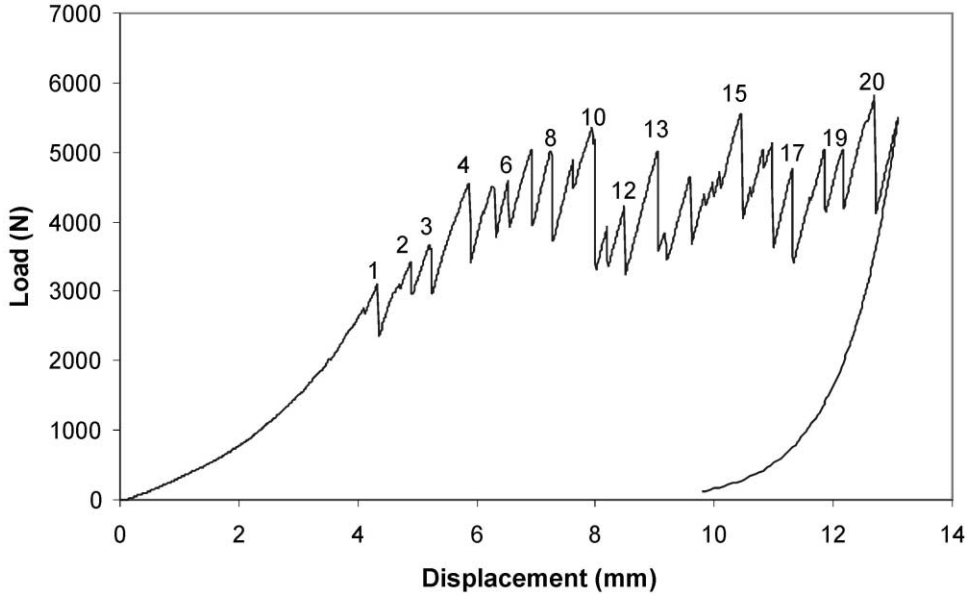

Fig. 8. Load vs. displacement for a DCB specimen. The 20 peak loads match 20 rows of broken stitches.

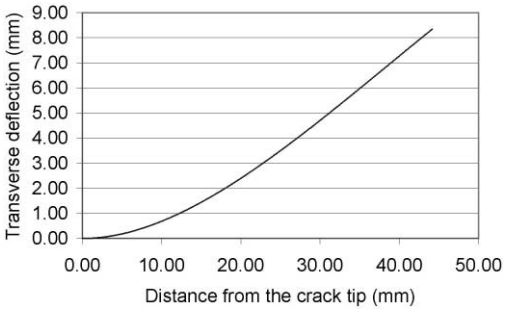

Fig. 10. Deflection curve of one arm of the DCB specimen at a load of 5420 N and crack length of 44.2 mm.

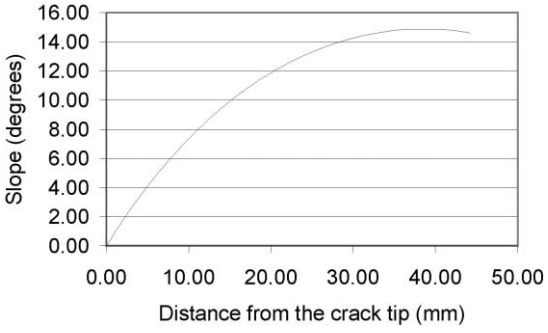

Fig. 11. The slope vs. distance from the crack tip for crack length = 44.2 mm and load = 5420 N.

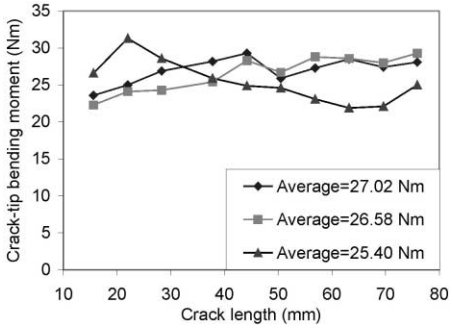

Fig. 12. Crack-tip bending moment variation as the crack propagates. Results for three specimens are shown.

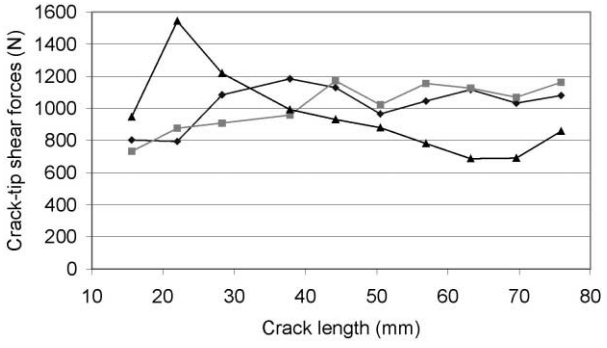

Fig. 13. Crack-tip shear forces vs. crack length for three specimens.

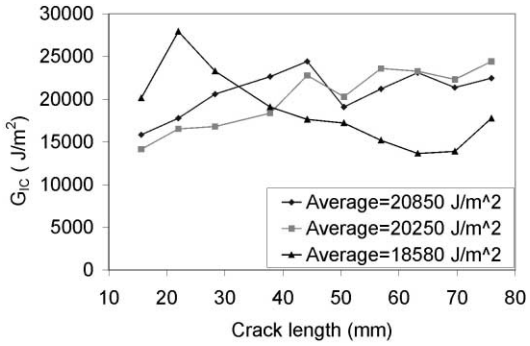

Fig. 14. The instantaneous G_{IC} of three specimens as a function of crack length.

reduces the compressive stresses and prevents micro buckling in the vicinity of the crack tip. The values of the bending moment can be used to calculate the critical strain energy release rate G_{IC} as shown in Eq. (6).

In Figs. 12–14 the crack-tip bending moment, shear force and G_{IC} are presented as a function of crack length for three different specimens. The average values for each specimen are shown in respective figures. The value of G_{IC} for unstitched specimen was found to be about 300 J/m^2 in a previous study [1]. Thus one can note that stitching has increased the apparent fracture toughness by a factor of about 60.

5. Conclusions

A new test method has been developed for measuring the Mode I fracture toughness of laminated composites containing medium to high density stitches. The fixture is designed such that a proportional axial force is applied to the specimen as the transverse forces on the DCB specimen increases. This prevents compressive failure of the specimen, and the crack propagates by breaking the stitches. The nonlinear differential equations of equilibrium are solved using an iterative process in order to determine the bending moment and shear force resultants for a given load and crack length. From the force resultants the critical energy release rate can be computed. The fracture toughness of the stitched graphite/epoxy specimens is found to be about 60 times that of unstitched specimens.

Acknowledgements

This research was supported by the NSF Grant 9732887 to the University of Florida. Partial support and stitched specimens were provided by the NASA Langley Research Center, Hampton, VA. The authors are thankful to Dr. D.R. Ambur and Mr. D.M. McGowan of NASA LaRC for their support and encouragement.

References

[1] Sharma SK, Sankar BV. Effects of Through-the Thickness Stitching on Impact and Interlaminar Fracture Properties of Textile Graphite/Epoxy Laminates. NASA Contractor Report 195042; February 1995.

[2] Dexter HB, Funk JG. Impact resistance and interlaminar fracture toughness of through-the thickness reinforced graphite/epoxy. AIAA paper 86-1020-CP; 1986. p. 700–9.

[3] Sankar BV, Zhu H. Effect of stitching on the low-velocity impact response of delaminated composite beams. Composites Science and Technology 2000;60:2681–91.

[4] Pelstring RM, Madan RC. Stitching to improve damage tolerance of composites 34th International SAMPE Symposium; May 1989. p. 1519–28.

[5] Mignery LA, Tan TM, Sun CT. The use of stitching to suppress delamination in laminated composites. ASTM STP 876, American Society for Testing and Materials, Philadelphia; 1985. p. 371–85.

[6] Ogo Y. The Effect of Stitching on In-plane and Interlaminar Properties of Carbon-epoxy Fabric Laminates. CCM Report Number 87-17, Center for Composite Materials, University of Delaware, Newark; May 1987. p. 1–188.

[7] Dransfield KA, Jain LK, Mai Y-W. On the effects of stitching in CFRPS-I. Mode I delamination toughness. Composites Science and Technology 1998;58(6):815–7.

[8] Sankar BV, Dharmapuri SM. Analysis of a stitched doubled Cantiliver beam. Journal of Composite Materials 1998;32(24): 2203–25.

[9] Sankar BV, Marrey RV. Analytical method for micromechanics of textile composites. Composites Science and Technology 1997; 57:703–13.

[10] Byun J, Gillespie JW, Chow T. Mode I delamination of a three-dimensional fabric composite. Journal of Composite Material 1990;24:497–518.

[11] Ridards R, Korjakin A. Interlaminar fracture toughness of GFRP influenced by fiber surface treatment. Journal of Composite Materials 1998;32(17):1528–59.

[12] Choi NS, Kinloch AJ, Williams JG. Delamination fracture of multidirectional carbon-fiber/epoxy composites under Mode I, Mode II and mixed-Mode I/II loading. Journal of Composite Materials 1999;33(1):73–100.

[13] Jain LK. On the effect of stitching on Mode 1 delamination toughness of laminated composites. Composites Science and Technology 1994;51:331–45.

[14] Sankar BV, Sonik V. Pointwise energy release rate in delaminated plates. AIAA Journal 1995;33(7):1312–8.

[15] Sankar BV, Sonik V. Modeling end-notched flexure tests of stitched laminates. Proceedings of the American Society for Composites Tenth Technical Conference, Technomic Publishing Co., Lancaster, Pennsylvania; 1995. p. 172–81.

[16] Chen L-S, Ifju PG, Sankar BV, Wallace B. A modified DCB test for composite laminates with high-density stitches. Proceedings of the American Society For Composites, Fourteenth Technical Conference, Bethel, CT; 27–29 September 1999. p. 214–7.

[17] Massabo R, Cox BN. Concepts for bridged mode II delamination cracks. Journal of the Mechanics and Physics of Solids 1999;47: 1265–300.